Original Article

Exploring the relationship between larmor-frequency electrical conductivity, diffusivity, and tissue volume in the aging brain

Taejun Park[1], Yunjeong Choi[2], Hyeok-Jae Kwon[3], Mun Bae Lee[4], Hak Young Rhee[5,6], Soonchan Park[1,6], Chang-Woo Ryu[1,6], Geon-Ho Jahng[1,6]^

[1]Department of Radiology, Kyung Hee University Hospital at Gangdong, Seoul, Republic of Korea; [2]Department of Biomedical Engineering, Undergraduate School, College of Electronics and Information, Kyung Hee University, Yongin-si, Republic of Korea; [3]Department of Chemistry, College of Basic Science, Yonsei University, Seoul, Republic of Korea; [4]Department of Mathematics, College of Basic Science, Konkuk University, Seoul, Republic of Korea; [5]Department of Neurology, Kyung Hee University Hospital at Gangdong, Seoul, Republic of Korea; [6]Department of Medicine, Kyung Hee University College of Medicine, Seoul, Republic of Korea

Contributions: (I) Conception and design: GH Jahng; (II) Administrative support: GH Jahng; (III) Provision of study materials or patients: HY Rhee, S Park, CW Ryu, GH Jahng; (IV) Collection and assembly of data: HY Rhee, GH Jahng; (V) Data analysis and interpretation: T Park, Y Choi, HJ Kwon, MB Lee, HY Rhee, GH Jahng; (VI) Manuscript writing: All authors; (VII) Final approval of manuscript: All authors.

Correspondence to: Geon-Ho Jahng, PhD. Department of Radiology, Kyung Hee University Hospital at Gangdong, Seoul, Republic of Korea; Department of Medicine, Kyung Hee University College of Medicine, 892 Dongnam-ro, Gangdong-Gu, Seoul 05278, Republic of Korea. Email: ghjahng@gmail.com.

Background: The aging brain undergoes various microstructural changes that influence its electrical properties. Conductivity, a measure of ion mobility, is particularly sensitive to these changes and can be assessed non-invasively using magnetic resonance electrical properties tomography (MREPT). Despite advancements in imaging techniques, the relationship between brain conductivity, diffusivity, and tissue volume in the context of aging and neurodegeneration remains incompletely understood. This study explores the relationships between electrical conductivity, diffusivity, and brain tissue volume in the aging brain, which is crucial for early diagnosis and monitoring of neurodegenerative diseases such as Alzheimer's, where these parameters could serve as potential biomarkers for disease progression.

Methods: In this cross-sectional, prospective study, 77 patients were assessed brain MREPT and diffusion tensor imaging with multiple shells and gradient directions (b=0, 800, and 2,000 s/mm^2). High-frequency conductivity (HFC) was calculated and separated into extra-neurite (EC) and intra-neurite conductivities (IC). We analyzed correlations between these conductivity indices and other magnetic resonance imaging (MRI) metrics, controlling for age, and explored the relationship between conductivity, diffusion, and Mini-Mental State Examination (MMSE) scores using multiple regression analysis.

Results: EC within the insular region negatively correlated with MMSE scores (r=–0.3027, P=0.0079). HFC in the hippocampus was positively associated with mean diffusivity (MD; β=192.4, P=0.008) and radial diffusivity (RD; β=207.6, P=0.004). HFC in the insula was positively associated with axial diffusivity (AxD; β=356.9, P=0.0004), MD (β=314.4, P=0.004), RD (β=275.5, P=0.012). EC in the hippocampus was positively associated with AxD (β=309.3, P=0.0001), MD (β=333.7, P<0.001), RD (β=341.8, P<0.001). EC in the insular was positively associated with AxD (β=324.1, P=0.0009) and MD (β=270.4, P=0.01). IC was positively correlated with intra-neurite diffusivity (ID) in the amygdala, thalamus, and insula.

Conclusions: These findings suggest that increased conductivity is associated with altered diffusivity and reduced cognitive performance, suggesting the use of MREPT to differentiate between conductivity changes

^ ORCID: 0000-0001-8881-1884.

due to ion mobility versus proton density, and how this approach contributes to understanding the aging brain and neurodegeneration. MREPT-derived measurements primarily reflect ion mobility and caution that clinical interpretations should consider the direct relationships between conductivity and diffusion changes.

Keywords: Magnetic resonance imaging (MRI); conductivity; diffusivity; brain tissue volume; aging brain
Submitted Oct 05, 2024. Accepted for publication Mar 12, 2025. Published online Apr 28, 2025.
doi: 10.21037/qims-24-2145
View this article at: https://dx.doi.org/10.21037/qims-24-2145

Introduction

Electrical or ionic conductivity is a physical parameter influenced by the movement of charges in response to an electric field. This movement is due to the motion of ionic charges (1), and is determined by the number of charged ions present and their respective charge. These factors are expressed in the formula

$$\sigma = qNM = \sum_{i}^{I} q_i N_i M_i \quad [1]$$

where σ is the conductivity, q represents the charge carried by the ions, N denotes the number of charged particles per unit volume (also known as concentration), and M signifies the mobility—the average velocity of a charge carrier when subjected to a unit electric field strength. Thus, conductivity escalates with increasing ion concentrations and ionic mobility. The total ionic conductivity represents the cumulative contribution of all free ions. Assessing the relationship between conductivity and variables such as mobility and ion concentrations through magnetic resonance imaging (MRI) *in vivo* is vital, as MRI systems are frequently employed to discern the conductivity characteristics under normal and abnormal bodily conditions.

Magnetic resonance electrical properties tomography (MREPT) is a noninvasive technique for mapping conductivity, which leverages standard MRI systems without the need for external electrodes or currents. It enables the imaging of conductivity at Larmor frequencies (approximately 128 MHz for a 3 Tesla MRI system), a parameter also known as high-frequency conductivity (HFC) (2). This electrical property is remarkably sensitive to an array of pathological and physiological conditions (3-8). Nonetheless, more investigative work is required to comprehend the underlying reasons for conductivity signal changes in pathological states using clinical MRI systems, particularly concerning the aforementioned relationship.

Within the imaging voxels obtained via an MRI system, it is possible to gauge the mobility of the imaged nuclei via diffusion measurements. Diffusivity quantifies the displacement of these nuclei over time. MRI is a common tool for assessing diffusivity in the human body through various indicators such as isotropic mean diffusivity (MD) and anisotropic fractional anisotropy (FA). Furthermore, diffusion is instrumental in modeling nervous tissue microstructures using techniques like the multi-compartment spherical mean technique (MC-SMT) (9) or neurite orientation dispersion and density imaging (NODDI) (10). Consequently, diffusion measurements performed with an MRI system can facilitate the evaluation of the relationship between conductivity and mobility. The association between diffusion of hydrogen spins (primarily water molecules) and conductivity at the Larmor frequency (~128 MHz) is not well established. At that frequency, the impedance measurement will have both a resistive component and a significant reactive component (mainly capacitive) due to cell membranes, etc. On the other hand, diffusion is not good at probing such conduction. Diffusion probes the mobility of protons whereas electrical conductivity probes the mobility of charged ions under the influence of electric fields.

In clinical practice, proton MRI is the standard. Proton signals can reflect proton concentration. Proton signals may be assessed through brain tissue volumes (BTVs), including gray matter volume (GMV), white matter volume (WMV), and cerebrospinal fluid (CSF) volume, typically derived from three-dimensional T1-weighted images (3D T1WIs). While sodium MRI (11) can map ion concentrations, a proton MRI system is challenging. In such cases, BTVs may be an alternative metric for assessing the relationship between conductivity and proton concentration inferred from BTVs in MRI signals. In neurodegenerative diseases, including Alzheimer's disease (AD), and in the aging brain, brain atrophy is a fundamental phenomenon caused by the loss of BTV. The areas affected by brain atrophy are often filled with CSF. Consequently, increased CSF volume leads to higher proton density in the atrophic regions and impacts increased conductivity. Additionally, in neurodegenerative diseases and aging brains, the breakdown or loosening of

brain tissue compartments results in increased diffusivity and a greater extracellular portion of protons. However, except in white matter bundles, we may assume that the total number of protons within an imaging voxel does not vary significantly, as the voxel size is typically large. In white matter bundles, if there is a loss of WMV, CSF can replace these areas, thereby altering compartmental conductivity.

The relationship between conductivity and cognitive decline appears to hinge on the movement of ions, which is influenced by brain microstructure changes. Conductivity is determined by ion mobility, which is affected by the diffusion of water molecules (12). Changes in the extracellular environment, which may occur due to atrophy or other structural alterations, facilitate ion movement (13,14). Thus, tissue changes that alter diffusivity (less dense environments, possibly due to atrophy or demyelination) are linked to altered conductivity. Conductivity changes are not only related to ion mobility but also to the structural integrity of brain tissue (15,16). For instance, in the intra-neurite space, the structured environment of axons with their cytoskeletal components facilitates the movement of ions and water molecules. Damage or disease can impair this structure, reducing both conductivity and diffusivity. The association between conductivity measures and cognitive decline could potentially happen due to underlying structural changes like increased diffusivity in certain brain regions.

We reviewed prior findings, particularly on MREPT applications in aging and neurodegeneration. MREPT can differentiate between normal and abnormal tissues by measuring conductivity (3,17). This ability to measure tissue conductivity makes MREPT a potential tool for identifying pathological changes in the brain associated with aging and neurodegenerative diseases. Studies have shown that MREPT measurements are repeatable and precise (18). This repeatability is crucial for longitudinal studies in aging and neurodegeneration, where consistent measurements over time are necessary. MREPT has been explored for its potential to be particularly useful in neurodegenerative diseases like AD and Parkinson's (7,12,19,20). Previous studies have shown elevated HFC and extra-neurite conductivity (EC) values in AD patients compared to cognitively normal (CN) and mildly cognitively impaired (MCI) participants (7,20). These findings are attributed to increased ion mobility rather than increased ion concentration due to brain tissue volume loss. This suggests that MREPT-derived conductivity measurements reflect changes in the brain's microenvironment associated with neurodegeneration. MREPT can help in early diagnosis and monitoring of disease progression by measuring changes in tissue conductivity. Neurodegenerative diseases are associated with mechanisms such as oxidative stress, protein misfolding, and chronic inflammation (21). MREPT can potentially provide insights into these molecular changes by measuring the electrical properties of brain tissues, offering a noninvasive way to study these conditions. MREPT can be used to monitor the effectiveness of therapeutic interventions by tracking changes in tissue conductivity over time. This application is particularly relevant for evaluating new treatments for neurodegenerative diseases (22).

To determine the relationship between conductivity and certain parameters using a clinical MRI system, we posed two primary questions: (I) How does diffusivity influence brain conductivity, and (II) How does proton density, indicated by brain tissue volumes, impact brain conductivity? To address these questions, we explored the relationship between conductivity and diffusivity, with the presumption that diffusion mirrors ionic mobility in MRI settings. Additionally, we investigated the correlation between conductivity and brain tissue volumes, positing that volumes such as GMV, WMV, and CSF volume serve as proxies for proton densities or concentrations within MRI signals, as opposed to direct ion concentration measurements. We hypothesized that conductivity measured via MREPT correlates with both diffusivity and brain tissue volumes. In pursuit of this hypothesis, we collected whole-brain MREPT data using a six-echo turbo spin-echo (TSE) pulse sequence from 77 older participants exhibiting a broad spectrum of cognitive functioning. We processed HFC data and further dissected HFC into compartmental conductivities of intra- and extra-neurite spaces using the MC-SMT model (9). We present this article in accordance with the STROBE reporting checklist (available at https://qims.amegroups.com/article/view/10.21037/qims-24-2145/rc).

Methods

Participants

This study was approved by the Institutional Review Board (IRB) of Kyung Hee University Hospital at Gangdong, Seoul, Republic of Korea (IRB No. khnmc2019-07-007), and all participants provided informed consent before their inclusion in this cross-sectional prospective study between August 2019 and December 2023. The study was conducted in accordance with the Declaration of Helsinki and its subsequent amendments. Participants were required to

submit a comprehensive medical history and were subjected to neurological examinations, standard neuropsychological tests, and MRI scanning. Global cognitive function was assessed using the Korean version of the Mini-Mental State Examination (K-MMSE) and the Clinical Dementia Rating (CDR). Cognitive capabilities were further evaluated through a comprehensive neuropsychological test battery standardized for Korean individuals, known as the Seoul Neuropsychological Screening Battery (23). The study encompassed a cohort of 77 older individuals, aged 74.9±5.8 years, with a male-to-female ratio of 24:53. The average score on the MMSE was 24.7±4.4. The scatter plot of MMSE scores versus age for all participants is shown in Figure S1.

MRI acquisition

A six-echo TSE pulse sequence was used (7) for the brain MREPT images with the repetition time (TR) =3,200 ms, first echo time (TE) =12 ms with 12 ms intervals, number of slices =20 without a gap between the slices, slice orientation = transverse, and acquired voxel size =2×2×5 mm^3. This is a multi-echo sequence. Therefore, the TSE factor was 6, indicating that the number of echoes was 6. The scan time of the MREPT sequence was 6 minutes and 5 seconds. We did not perform MREPT measurements using TSE with two different polarities of imaging gradients to reduce eddy currents because of limiting scan time in elderly participants (24). Real and imaginary images were saved to reconstruct the conductivity map.

A single-shot spin-echo echo-planner imaging (SS-SE-EPI) pulse sequence was used to obtain diffusion tensor to model the MC-SMT (9) with two *b*-shells of nominally 800 and 2,000 s/mm^2 with 16 and 32 gradient directions of diffusion tensor, respectively. The imaging parameters were TR/TE =15,000/86 ms and voxel size =2×2×2 mm^3. Total scan times were 2 minutes 15 s, 4 minutes 45 s, and 8 minutes 45 s for b-values of 0, 800, and 2,000 s/mm^2, respectively.

Finally, a sagittal structural 3D T1WI was acquired with the fast field-echo (FFE) sequence for image registration and brain tissue segmentation with the voxel size of 1×1×1 mm^3. In addition, T2-weighted turbo-spin-echo, fluid-attenuated inversion recovery (FLAIR), and gradient-echo images were also acquired to evaluate any brain abnormalities. MRI was performed using a 3.0 Tesla MRI system equipped with a 32-channel sensitivity encoding head coil (Ingenia, Philips Medical System, Best, The Netherlands).

Reconstruction of acquired MRI data

We first mapped HFC from MREPT, then applied MC-SMT to derive extra-neurite and intra-neurite compartment information from multi-shell diffusion tensor data, and calculated compartmental conductivities and diffusivities. We explained how to reconstruct images, shortly (12,25,26).

First, to obtain HFC, we used the double derivative of the B1 field equation:

$$\nabla^2 B_1 = i\omega\mu_0\,\tau_H B_1 - \frac{\nabla\tau_H}{\tau_H}\times(\nabla\times B_1) \quad [2]$$

where B_1 is the B1 field, ω is the angular frequency, $\mu_0 = 4\pi\times10^{-7}\,N/A^2$ is the magnetic permeability of the free space, and $\tau_H = \sigma_H + i\omega\epsilon_H$ is the high-frequency electrical tissue properties of HFC σ_H and permittivity ϵ_H (2). With the phase term ϕ^+ (ϕ^+) of the positive (negative) rotating component of the transverse field of B_1, a phase-based MREPT formula with the regularization coefficient *c*, was derived as:

$$-c\nabla^2\left(\frac{1}{\sigma_H}\right)+\left(\nabla\phi^{tr}\cdot\nabla\left(\frac{1}{\sigma_H}\right)\right)+\frac{\nabla^2\phi^{tr}}{\sigma_H}=2\omega\mu_0 \quad [3]$$

Where $\phi^{tr}=\phi^+ + \phi^-$ is the measurable transceiver phase using MRI (25). To solve the partial differential equation in Eq. [3], we used the 2-dimensional finite-difference method. For each image matrix, Eq. [3] is written as:

$$\begin{bmatrix} \vdots \\ -c\left(\frac{\partial^2}{\partial x^2}+\frac{\partial^2}{\partial y^2}\right)+\frac{\partial\phi^{tr}}{\partial x}\frac{\partial}{\partial x}+\frac{\partial\phi^{tr}}{\partial y}\frac{\partial}{\partial y}+\frac{\partial^2\phi^{tr}}{\partial x^2}+\frac{\partial^2\phi^{tr}}{\partial y^2} \\ \vdots \end{bmatrix}\begin{bmatrix} \vdots \\ \frac{1}{\sigma_H} \\ \vdots \end{bmatrix}=\begin{bmatrix} \vdots \\ 2\omega\mu_0 \\ \vdots \end{bmatrix} \quad [4]$$

The finite-difference method for solving the equation is to find the solutions of a linear matrix system $\mathbf{Ax}=\mathbf{b}$ with the appropriate processing of the Dirichlet boundary conditions (σ_H =0.5 S/m). $\mathbf{A}$ is a staff matrix, $\mathbf{x}=\left(\frac{1}{\sigma_{H_1}},\frac{1}{\sigma_{H_2}},\cdots,\frac{1}{\sigma_{H_N}}\right)$, and $\mathbf{b}=(2\omega\mu_0, 2\omega\mu_0, \ldots, 2\omega\mu_0)$, respectively. We used the finite-difference method to solve the above matrix system with regularization coefficient $c = -0.03$ in Eq. [3].

Second, the recovered HFC σ_H was decomposed into the intra-neurite and extra-neurite compartments to calculate the compartmental conductivities (27-30):

$$\sigma_H = \sigma_{int} + \sigma_{ext} = v_{int}\,c^{int}\,D^{int} + (1-v_{int})\,c^{ext}\,D^{ext} \quad [5]$$

where σ_{int} and σ_{ext} are the intra-neurite conductivity (IC) and the EC, respectively, v_{int} is the intra-neurite volume fraction (IVF), c^{int} is the intra-neurite ion concentration and c^{ext} is the extra-neurite ion concentration (EIC). Similarly, D^{int} and D^{ext} are the intra-neurite diffusivity (ID) and the

extra-neurite diffusivity (ED), respectively. To obtain v_{int}, D^{int} and D^{ext} in Eq. [5], we used the MC-SMT (9) software (https://ekaden.github.io). Using the reference value β =0.41 (30), the ratio of ion concentrations in the intra- and extra-compartments was set as $c^{int} = \beta c^{ext}$ and then by using Eq. [5], D^{ext} can be expressed as the following form (27-30):

$$c^{ext} = \frac{\sigma_H}{v_{int}\beta D^{int} + (1 - v_{int}) D^{ext}} \quad [6]$$

Using MREPT and MC-SMT data, we obtained the following parameter maps: HFC and two separated conductivities of EC and IC, two diffusivities of ED and ID, EIC, and IVF. These maps were further processed with the 3D T1WI in the following step.

The intra-neurite diffusivity in intracellular volume (ID_IV) and the extra-neurite diffusivity in extracellular volume (ED_EV) were calculated by ID·IVF and ED (1-IVF), respectively. Furthermore, ED_EV_WM and ID_IV_WM were ED_EV and ID_IV for voxels that contained greater than 20% WMV, respectively. Finally, a 3×3 diffusion tensor with three eigenvalues ($\lambda_1 \geq \lambda_2 \geq \lambda_3$) was calculated using diffusion tensor imaging (DTI) data of b =800 s/mm^2. The several diffusion indices, such as axial diffusivity (AxD or ADC) which is λ_1, radial diffusivity (RD) which is $(\lambda_2 + \lambda_3)/2$, MD and FA, were also calculated using the eigenvalues of the diffusion tensor.

Post-processing of all reconstructed maps

The 3D T1WI was spatially normalized into an AD-specific brain template (31) and segmented into GMV, WMV, and CSFV using the computational anatomy toolbox (CAT12) tool (http://www.neuro.uni-jena.de/cat/). All created maps were then spatially normalized into the brain template using the deformation field information from the 3D T1WI. Gaussian smoothing using the full-width at half maximum (FWHM) of 10×10×10 mm^3 was applied to all parameter maps for voxel-based statistical analyses. To process the reconstructed maps of each participant, the Statistical Parametric Mapping version 12 (SPM12) software (http://www.fil.ion.ucl.ac.uk/spm/software/spm12/) was used.

Statistical analysis of maps

Voxel-based multiple regression analyses

We performed voxel-based multiple regression analyses to examine the associations between each map and variables including age and Mini-Mental State Examination (MMSE) scores, with age as a covariate.

Therefore, we evaluated the following model for age: $\text{Conductivity or diffusivity maps} \approx \beta_1 * age + error$ and for MMSE score: $\text{Conductivity or diffusivity maps} \approx \beta_1 * age + \beta_2 * MMSE\ score + error$. For these analyses, a significance threshold of α=0.05 with corrections for multiple comparisons was employed via the false discovery rate (FDR) method. Only clusters comprising a minimum of 100 contiguous voxels were considered significant.

Region of interest (ROI)-based analyses

Atlas-based ROI areas were identified in brain regions commonly affected by AD, including the hippocampus [0102], amygdala [0506], thalamus [1314], insula [2425], and corpus callosum [28], using the wfu_pickatlas software (http://fmri.wfubmc.edu/software/PickAtlas). We selected these ROIs—numbered solely for convenience—to extract values from each spatially normalized map across all participants. Data extraction was performed with Marsbar software (Matthew Brett, http://marsbar.sourceforge.net).

We then conducted a Pearson correlation heatmap analysis to explore potential correlations between conductivity indices, BTVs, and diffusion indices. Additionally, we performed a partial correlation analysis, controlling for age, to investigate the relationships between conductivity or diffusion indices within each ROI and MMSE score.

A stepwise multiple regression analysis, including variables with P<0.1 and excluding those with P>0.1, was utilized to assess the association between conductivity values, BTVs, and diffusion index values while controlling for age and MMSE scores. The model was formulated as follows:

$$\begin{aligned}\text{Conductivity} \approx \beta_1 * \text{age} + \beta_2 * \text{MMSE} + \beta_3 * \text{each BTV index} \\ + \beta_4 * \text{each diffusion index} + \text{error}\end{aligned} \quad [7]$$

where conductivity represents one of conductivity indices such as HFC, EC, EC_WM, IC, and IC_WM, BTV pertains to one of the brain tissue volumes such as CSF volume, GMV, or WMV, and diffusion index refers to one of the diffusion indices such as (AxD or ADC), MD, FA, RD, ED, ED_EV, ED_EV_WM, ID, ID_IV, and ID_IV_WM. Based on a robust positive correlation highlighted by the heatmap analysis, we selected the relevant indices for each model. The models, each adjusted for multiple testing, were rigorously tested across ROIs:

(I) For HFC and EC, we considered diffusion indices (AxD, MD, RD, ED_EV) alongside CSF volume, resulting in four tested models for each ROI.

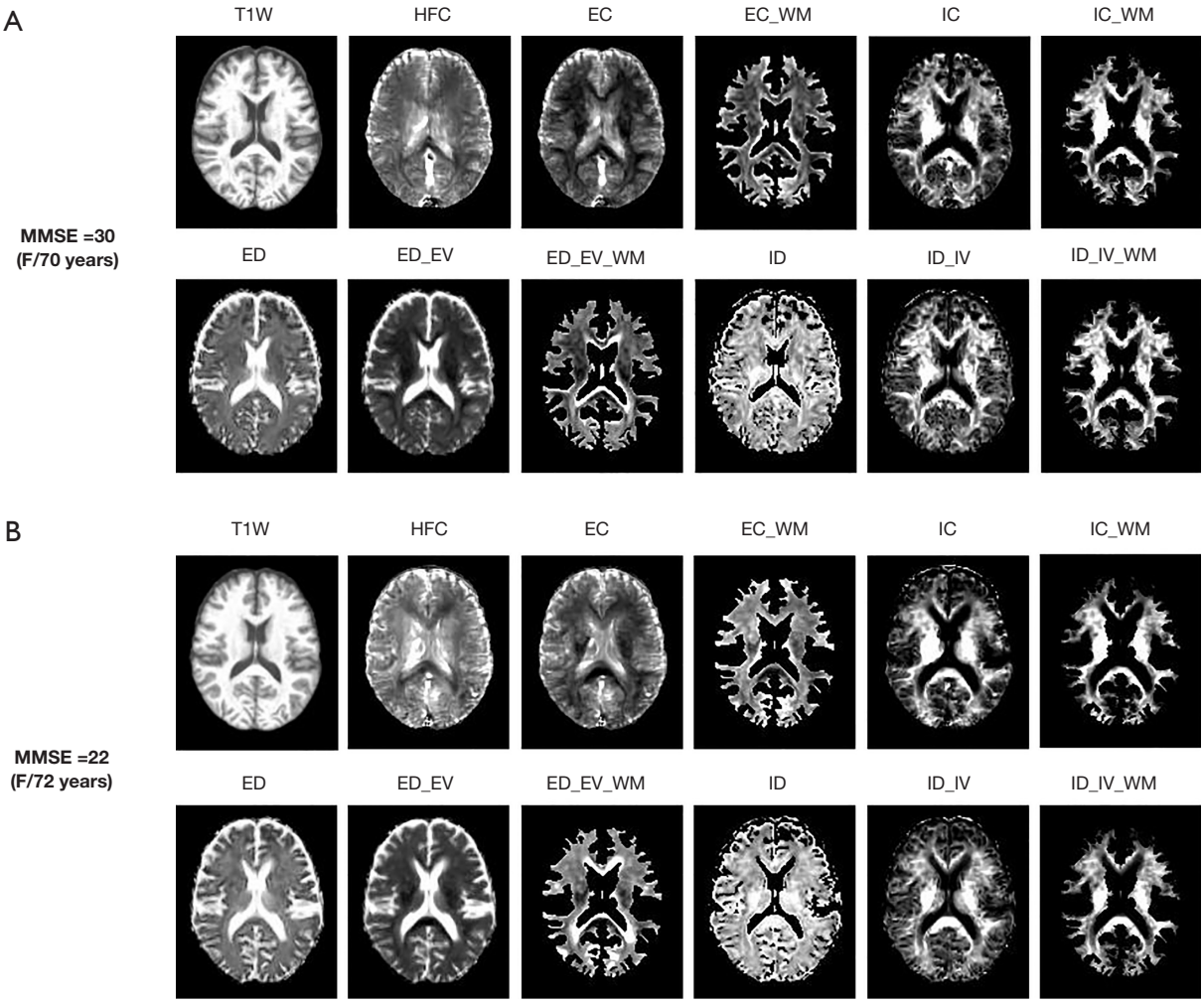

Figure 1 Representative conductivity maps calculated with MREPT and the corresponding diffusion maps calculated with MC-SMT obtained from two participants who had MMSE score =30 and MMSE score =22. EC, extra-neurite conductivity; ED, extra-neurite diffusivity; EV, extracelluar volume; HFC, high-frequency conductivity; IC, intra-neurite conductivity; ID, intra-neurite diffusivity; IV, intracellular volume; MC-SMT, multi-compartment spherical mean technique; MMSE, Mini-Mental State Examination; MREPT, magnetic resonance electrical properties tomography; WM, white matter.

A significance level of $\alpha<0.0125$ (adjusted from $\alpha=0.05$ for four models) was implemented for each comparison.

(II) For EC_WM, the analysis incorporated the diffusion index ED_EV_WM and BTVs of WMV and CSF volume. Two models were tested for each ROI, with a significance level of $\alpha<0.025$ (adjusted from $\alpha=0.05$ for two models).

(III) For both IC and IC_WM, we included diffusion indices (ID, ID_IV, and ID_IV_WM) and WMV. Three models were tested per ROI, with a significance level of $\alpha<0.0167$ (adjusted from $\alpha=0.05$ for three models).

These analytical approaches allowed us to rigorously probe the associations and interactions between conductivity and the various anatomical and physiological indices obtained from MRI scans.

Results

Figure 1 illustrates exemplary conductivity maps derived via MREPT alongside corresponding diffusion maps generated through MC-SMT. These maps represent two participants, one with a high MMSE score of 30 and the other with a

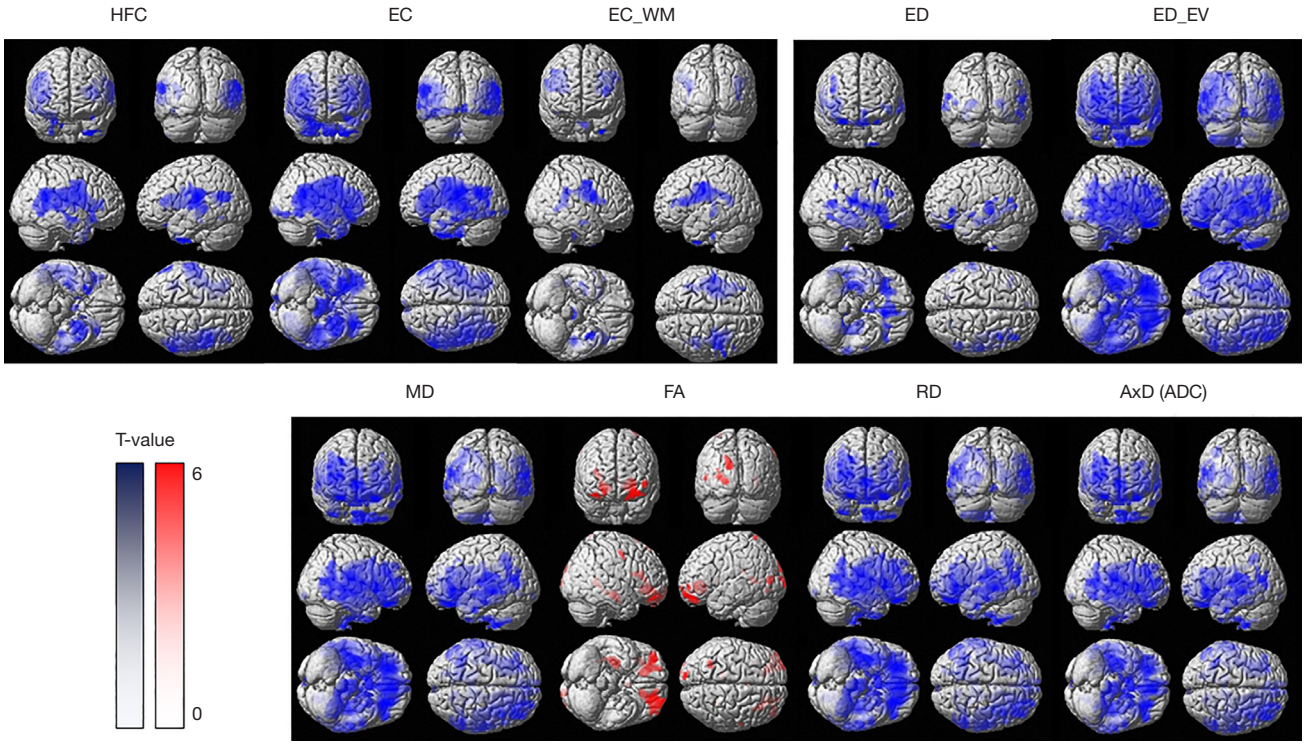

Figure 2 Results of voxel-based multiple regression analysis between conductivity or diffusion maps and MMSE score with age as a covariate. We evaluated the following multiple-regression model for age: Conductivity or diffusivity maps ≈β1*age + *error* and for MMSE score: Conductivity or diffusivity maps ≈β1*age + β2*MMSE score + *error*. The red and blue colors represent positive and negative associations, respectively. Age did not correlate with any conductivity indices. AxD (ADC), axial diffusivity; EC, extra-neurite conductivity; ED, extra-neurite diffusivity; EV, extracellular volume; FA, fractional anisotropy; HFC, high-frequency conductivity; MD, mean diffusivity; MMSE, mini-mental state examination; RD, radial diffusivity; WM, white matter.

lower score of 22. The imaging window level was identically adjusted for both cases. Visually discerning differences between the maps for each participant proved challenging.

Voxel-based analyses

Figure 2 depicts the results of voxel-based multiple regression analysis probing the relationship between conductivity or diffusion maps and MMSE scores. A significant negative correlation was found with MMSE scores for the following conductivity metrics: HFC, EC, and EC_WM. This implies that an increase in these values is associated with cognitive deterioration. Specifically, the HFC-related regions included the left postcentral gyrus, left precentral gyrus, right supramarginal gyrus, right insula, left middle temporal gyrus, left parahippocampal gyrus, left inferior frontal gyrus, and left fusiform gyrus. For EC, the implicated areas were the frontal lobe white matter and lingual gyri bilaterally. White matter regions in the frontal and temporal lobes and the left insula were associated with EC_WM. A detailed account of these areas can be found in Table S1. However, IC and IC_WM showed no significant relationship with MMSE scores, nor did age correlate with any conductivity indices.

Diffusion indices such as ED and ED_EV derived from MC-SMT and MD, RD, and AxD derived from DTI exhibited a significant negative correlation with MMSE scores, while FA showed a significant positive correlation. These associations are summarized in Table S2. No significant correlations were found between age and any diffusion indices.

ROI-based analyses

Correlation analysis between conductivity or diffusion and MMSE scores

Mirroring the voxel-based findings, the ROI-based correlation analysis also examined the relationships between conductivity or diffusion values and MMSE scores

Table 1 Results of the partial correlation analysis between ROI values obtained from all the participants in each brain area and MMSE scores

Brain areas	Amygdala		Corpus callosum		Hippocampus		Insula		Thalamus	
	r	P value	r	P value	r	P value	r	P value	r	P value
Conductivity indices										
HFC	−0.2246	0.0511	−0.08370	0.4723	−0.1069	0.3581	−0.2739	0.0167	0.007098	0.9515
EC	−0.1972	0.0878	−0.2248	0.0509	−0.09434	0.4176	−0.3027*	0.0079*	−0.01909	0.8700
EC_WM	−0.1054	0.3651	−0.1498	0.1964	0.05443	0.6405	−0.2779*	0.0151*	0.006490	0.9556
IC	−0.03244	0.7809	0.2228	0.0530	0.1626	0.1605	0.07746	0.5060	0.04257	0.7150
IC_WM	−0.01475	0.8994	0.2495*	0.0297*	0.1436	0.2159	0.1248	0.2827	0.06374	0.5844
Diffusion indices										
MD	−0.2189	0.0575	−0.2229	0.0530	−0.2789*	0.0147*	−0.2969*	0.0092*	−0.2525*	0.0278*
FA	−0.07502	0.5195	0.2485*	0.0304*	0.2290*	0.0466*	−0.1409	0.2247	0.07135	0.5402
RD	−0.2045	0.0764	−0.2322*	0.0436*	−0.2790*	0.0147*	−0.2832*	0.0132*	−0.2392	0.0374
AxD (ADC)	−0.2363*	0.0399*	−0.1896	0.1009	−0.2768*	0.0155*	−0.3184*	0.0051*	−0.2749*	0.0162*
ED	−0.2182	0.0583	−0.1562	0.1779	−0.2255	0.0502	−0.2988*	0.0087*	−0.2321*	0.0436*
ED_EV	−0.2637*	0.0214*	−0.2207	0.0554	−0.2322*	0.0436*	−0.3581*	0.0015*	−0.2489*	0.0301*
ED_EV_WM	−0.2353*	0.0407*	−0.1521	0.1897	−0.06269	0.5906	−0.2317*	0.0440*	−0.1103	0.3430
ID	−0.1630	0.1595	0.05656	0.6275	−0.1950	0.0915	−0.1679	0.1472	−0.1627	0.1601
ID_IV	−0.02364	0.8394	0.2634*	0.0215*	0.1436	0.2160	0.08385	0.4714	−0.04444	0.7030
ID_IV_WM	−0.06232	0.5928	0.2917*	0.0106*	0.1362	0.2409	0.1048	0.3677	−0.01355	0.9075

The partial correlation analysis was performed with age as a covariate. Data are listed as the partial correlation coefficient rho with the P value. The significant level is α=0.008 (α=0.05 divided by 6 ROIs). Atlas-based ROIs were defined at the hippocampus, parahippocampal gyrus (Parahippo), middle temporal gyrus (Mid TG), middle frontal gyrus (Mid FG), and middle occipital gyrus (Mid OG). *, a significant correlation between MRI measures and MMSE scores. ADC, axial diffusivity; EC, extra-neurite conductivity; ED, extra-neurite diffusivity; EV, extracellular volume; FA, fractional anisotropy; HFC, high-frequency conductivity; IC, intra-neurite conductivity; ID, intra-neurite diffusivity; IV, intracellular volume; MD, mean diffusivity; MMSE, Mini-Mental State Examination; RD, radial diffusivity; ROI, region of interest; WM, white matter.

within predefined brain areas. The results are concisely presented in *Table 1*. Conductivity measurements in the insula, specifically EC (r=−0.3027, P=0.0079) and EC_WM (r=−0.2779, P=0.0151), were found to have a significant negative correlation with MMSE scores. Conversely, IC_WM within the corpus callosum was significantly positively correlated with MMSE scores (r=0.2495, P=0.0297). Diffusion metrics, such as MD, RD, AxD, ED_EV, and ED_EV_WM, showed negative correlations in certain ROIs, whereas FA, ID_IV, and ID_IV_WM had positive correlations with MMSE scores across select regions.

Correlation analysis between conductivity and diffusivity or BTV using the heatmap

Figure 3 presents the correlation heatmap revealing the interplay between conductivity values and either diffusion metrics or BTV in each ROI. The heatmap's Y-axis represents conductivity indices, while the left side of the X-axis lists BTV indices, and the middle to right side displays diffusivity indices. A reddish hue denotes positive correlations, and bluish indicates negative ones. Both IC_WM and IC exhibited positive correlations with diffusion indices such as ID_IV and ID, along with WMV in the BTV category. EC_WM showed a positive link with the diffusion index ED_EV_WM and WMV. Similarly, EC and HFC had positive correlations with diffusivity indices, including ED_EV, ED, RD, MD, and AxD, and with CSF volume in the BTV category. These positive associations were the basis for selection in the following multiple regression models.

Multiple regression analysis

The results of the multiple regression analyses are

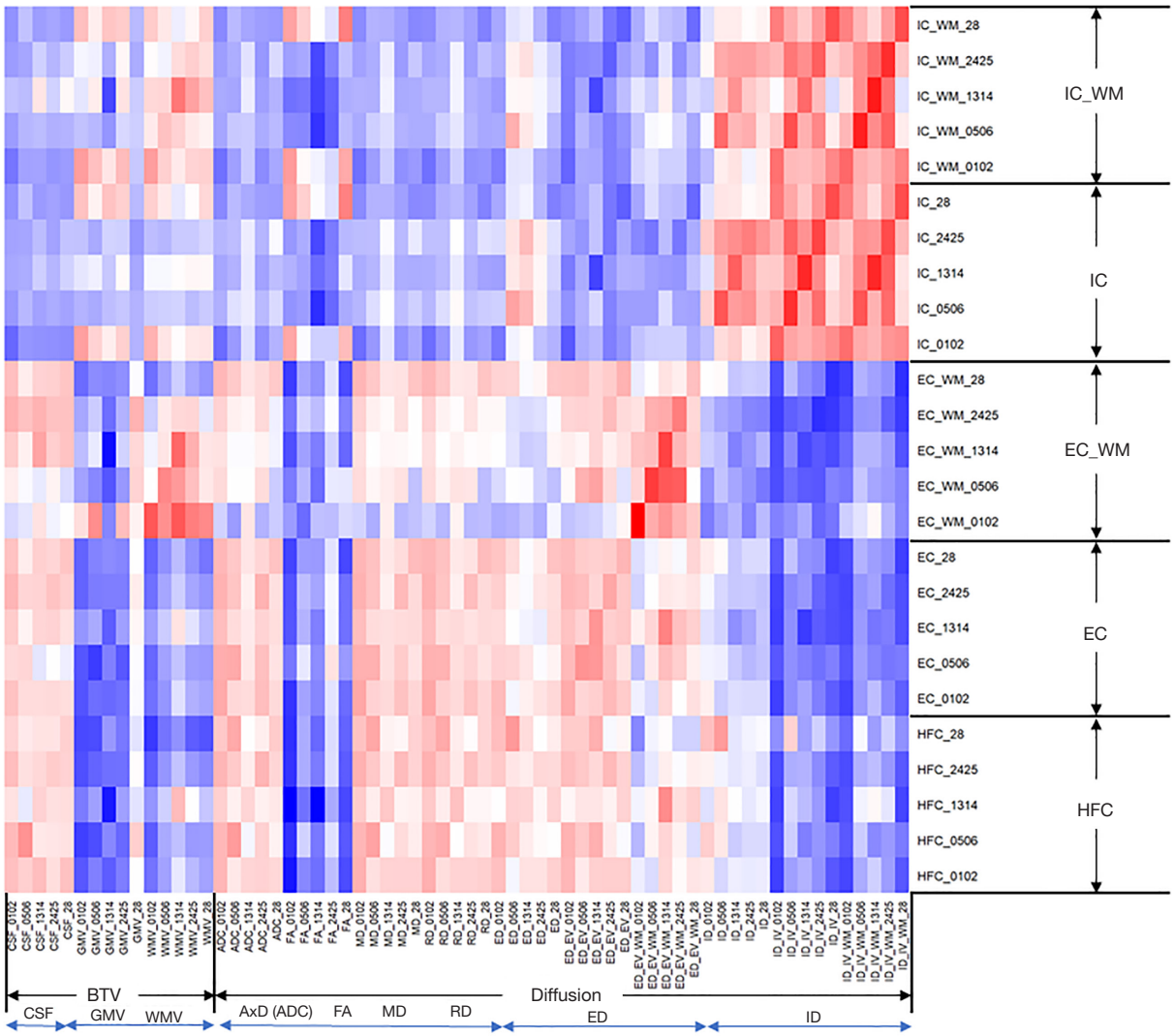

Figure 3 Result of correlation analysis between conductivity values and diffusion or BTV values in each ROI using the heatmap method. The Y-axis indicates conductivity indices and the X-axis indicates brain tissue volume indices of CSF, GMV, and WMV (left side) and diffusion indices (middle and right side). The red color indicates a positive correlation and the blue color indicates a negative correlation. The number indicates the atlas-based ROI areas as the hippocampus [0102], amygdala [0506], thalamus [1314], insular [2425], and corpus callosum [28] without separate left and right brain sides. AxD (ADC), axial diffusivity; BTV, brain tissue volume; CSF, cerebrospinal fluid volume; EC, extra-neurite conductivity; ED, extra-neurite diffusivity; EV, extracellular volume; FA, fractional anisotropy; GMV, gray matter volume; HFC, high-frequency conductivity; IC, intra-neurite conductivity; ID, intra-neurite diffusivity; IV, intracellular volume; MD, mean diffusivity; RD, radial diffusivity; ROI, region of interest; WM, white matter; WMV, white matter volume.

detailed in *Tables 2-4* and Tables S3-S6. *Table 2* outlines the association between HFC with diffusivity metrics and the BTV index of CSF volume across ROIs. The models proved significant per analysis of variance (ANOVA) assessment, except in the corpus callosum. Neither age nor MMSE scores were substantially tied to HFC in any ROI. CSF volume bore no significant relation to HFC, except for the amygdala when accounting for ED_EV. Significant associations were found between HFC and MD, RD in the hippocampus, and AxD, MD, RD, ED_EV in the insula. The result of the association between HFC with diffusivity metrics and the BTV index of GMV volume across ROIs is

Table 2 Result of multiple regression analysis between HFC and diffusion indices and CSF BTV index

HFC and ROI	Age (β/P)	MMSE (β/P)	Diffusion (β/P)	CSF BTV (β/P)	ANOVA (F/P)
Hippocampus					
AxD	−0.001/0.709	0.002/0.444	158.6/0.025	0.150/0.289	10.03/<0.0001
MD	−0.001/0.721	0.002/0.436	192.4/0.008*	0.089/0.532	10.83/<0.0001
RD	−0.0005/0.731	0.002/0.433	207.6/0.004*	0.062/0.666	11.28/<0.0001
ED EV	−0.001/0.497	0.001/0.590	157.9/0.027	0.139/0.347	9.991/<0.0001
Amygdala					
AxD	0.002/0.408	−0.002/0.481	269.4/0.089	1.777/0.040	6.936/0.0001
MD	0.002/0.390	−0.003/0.470	276.6/0.115	1.916/0.023	6.791/0.0001
RD	0.002/0.378	−0.003/0.464	263.6/0.146	2.031/0.014	6.664/0.0001
ED EV	0.002/0.332	−0.002/0.547	135.8/0.260	2.329/0.003*	6.374/0.0002
Thalamus					
AxD	0.0004/0.847	0.003/0.232	204.6/0.059	1.140/0.030	3.716/0.008
MD	0.0004/0.818	0.003/0.209	243.8/0.019	1.101/0.031	4.304/0.004
RD	0.0004/0.824	0.003/0.204	256.3/0.011*	1.097/0.029	4.600/0.002
ED EV	−0.001/0.722	0.003/0.224	181.7/0.041	1.249/0.013	3.898/0.006
Insula					
AxD	−0.001/0.500	−0.001/0.422	356.9/0.0004*	0.068/0.754	13.53/<0.0001
MD	−0.001/0.536	−0.002/0.307	314.4/0.004*	0.069/0.748	11.82/<0.0001
RD	−0.001/0.583	−0.002/0.261	275.5/0.012*	0.160/0.448	10.95/<0.0001
ED EV	<0.0001/0.950	−0.001/0.555	301.9/0.001*	0.130/0.480	12.60/<0.0001
Corpus callosum					
AxD	0.002/0.347	−0.001/0.790	83.42/0.319	0.091/0.362	1.592/0.186
MD	0.002/0.327	−0.001/0.799	61.61/0.414	0.094/0.373	1.503/0.210
RD	0.002/0.323	−0.001/0.796	50.51/0.472	0.098/0.357	1.463/0.223
ED EV	0.002/0.338	−0.001/0.735	7.624/0.888	0.135/0.218	1.327/0.268

In this analysis, we used the model as HFC ≈ β1 * age + β2 * MMSE + β3 * diffusion index + β4 * CSF BTV index + ε (error). For the diffusion indices, we used AxD (ADC), MD, RD, and ED at EV. For the BTV index, we used CSF volume. Therefore, the four tested models were ADC and CSF, MD and CSF, RD and CSF, and ED_EV and CSF for each ROI. For each ROI, $\alpha<0.05$ divided by 4 tested models (0.05/4=0.0125) was used to determine the significance level. *, significant association between conductivity value and other indices. AxD (ADC), axial diffusivity; ANOVA, analysis of variance; BTV, boundary tissue volume; CSF, cerebrospinal fluid; ED, extra-neurite diffusivity; EV, extracellular volume; HFC, high-frequency conductivity; MD, mean diffusivity; MMSE, mini-mental state examination; RD, radial diffusivity; ROI, region of interest.

listed in Table S3.

Table 3 reports the association between EC and diffusivity metrics along with the BTV index of CSF volume. Significance prevailed across all ROIs per ANOVA, including the corpus callosum. Age and MMSE scores had no meaningful influence on EC values. CSF volume was unrelated to EC except in the corpus callosum with AxD. Noteworthy associations with EC were MD, RD, and ED_EV in the hippocampus; AxD and ED_EV in the amygdala; ED_EV in the thalamus; AxD, MD, and ED_EV in the insula; and AxD, MD, RD, and ED_EV in the corpus callosum. The result of the association between EC with diffusivity metrics and the BTV index of GMV volume across ROIs is listed in Table S4. Table S5 explains

Table 3 Result of multiple regression analysis between EC and diffusion indices, and CSF BTV index

EC and ROI	Age (β/P)	MMSE (β/P)	Diffusion (β/P)	CSF BTV (β/P)	ANOVA (F/P)
Hippocampus					
AxD	−0.0003/0.824	0.002/0.360	309.3/0.0001*	−0.076/0.605	13.93/<0.0001
MD	−0.0003/0.856	0.002/0.355	333.7/<0.0001*	−0.122/0.414	14.72/<0.0001
RD	−0.0002/0.877	0.002/0.355	341.8/<0.0001*	−0.138/0.357	15.04/<0.0001
ED EV	−0.001/0.442	0.001/0.617	296.8/0.0001*	−0.079/0.611	13.23/<0.0001
Amygdala					
AxD	0.002/0.467	−0.003/0.284	379.8*/0.009*	−0.263/0.735	4.165/0.004
MD	0.002/0.438	−0.003/0.274	394.4/0.015	−0.078/0.918	3.900/0.006
RD	0.002/0.420	−0.004/0.269	381.0/0.023	0.073/0.921	3.669/0.009
ED EV	0.002/0.276	−0.002/0.472	378.8/0.0005*	0.030/0.963	5.906/0.0004
Thalamus					
AxD	0.002/0.363	0.002/0.397	145.3/0.144	1.065/0.028	2.918/0.027
MD	0.002/0.328	0.002/0.365	181.8/0.058	1.022/0.030	3.351/0.014
RD	0.002/0.322	0.002/0.356	194.7/0.037	1.013/0.030	3.583/0.010
ED EV	0.001/0.499	0.003/0.107	366.1/<0.0001*	0.782/0.050	10.02/<0.0001
Insula					
AxD	−0.001/0.462	−0.002/0.273	324.1*/0.0009*	0.027/0.898	15.22/<0.0001
MD	−0.001/0.518	−0.002/0.190	270.4/0.010*	0.176/0.397	13.27/<0.0001
RD	−0.001/0.573	−0.002/0.160	227.3/0.032	0.270/0.187	12.37/<0.0001
ED EV	−<0.0001/0.981	−0.001/0.563	403.0/<0.0001*	0.003/0.988	20.45/<0.0001
Corpus callosum					
AxD	−0.0003/0.813	−0.002/0.317	180.3/0.006*	0.213/0.007*	10.08/<0.0001
MD	−0.0001/0.927	−0.002/0.376	174.9/0.003*	0.184/0.023	10.59/<0.0001
RD	−<0.0001/0.977	−0.001/0.395	163.2/0.003*	0.178/0.029	10.63/<0.0001
ED EV	0.0006/0.659	−0.001/0.384	145.7/0.0005*	0.144/0.076	12.00/<0.0001

In this analysis, we used the model as EC ≈ β1 * age + β2 * MMSE + β3 * diffusion index + β4 * CSF BTV index + ε (error). For the diffusion indices, we used AxD (ADC), MD, RD, and ED at EV. For the BTV index, we used CSF volume. Therefore, the four tested models were ADC and CSF, MD and CSF, RD and CSF, and ED_EV and CSF for each ROI. For EC ROI, $\alpha<0.05$ divided by 4 tested models (0.05/4=0.0125) was used to determine the significance level. *, significant association between conductivity value and other indices. AxD (ADC), axial diffusivity; ANOVA, analysis of variance; BTV, boundary tissue volume; CSF, cerebrospinal fluid; EC, extra-neurite conductivity; ED, extra-neurite diffusivity; EV, extracellular volume; MD, mean diffusivity; MMSE, mini-mental state examination; RD, radial diffusivity; ROI, region of interest.

the association between EC_WM and the diffusion index ED_EV_WM alongside BTV indices of WMV and CSF volume. The significance of the regression models spanned all ROIs. No substantial association existed between age, MMSE scores, and EC_WM. WMV was linked significantly to EC_WM in the hippocampus and thalamus ROIs, while CSF volume was associated with the insula and corpus callosum. ED_EV_WM strongly corresponded with EC_WM across all ROIs.

Table 4 delineates the associations with IC, diffusivity metrics, and WMV as the BTV index. All models achieved significance in every ROI investigated. Neither age nor MMSE scores notably influenced IC. WMV was significantly associated with IC in the hippocampus,

Table 4 Result of multiple regression analysis between IC and diffusion indices and WMV BTV index

IC and ROI	Age (β/P)	MMSE (β/P)	Diffusion (β/P)	WMV BTV (β/P)	ANOVA (F/P)
Hippocampus					
ID	−0.0003/0.444	0.0005/0.399	−1.366/0.942	0.477/0.001*	5.530/0.001
ID IV	−0.0002/0.307	0.0002/0.587	148.5/<0.0001*	0.071/0.344	60.23/<0.0001
ID IV WM	−0.0003/0.335	0.0004/0.338	416.6/<0.0001*	−0.177/0.082	41.23/<0.0001
Amygdala					
ID	0.0004/0.428	0.0008/0.269	113.4/<0.0001*	0.235/0.188	18.66/<0.0001
ID IV	0.0003/0.464	−<0.0001/0.873	187.1/<0.0001*	0.061/0.681	34.92/<0.0001
ID IV WM	0.0003/0.583	−<0.0001/0.979	661.8/0.0001*	−0.535/0.005*	21.86/<0.0001
Thalamus					
ID	0.0002/0.800	0.002/0.060	152.5/<0.0001*	0.282/0.006*	24.87/<0.0001
ID IV	0.0003/0.553	0.001/0.159	213.6/<0.0001*	0.271/<0.0001*	86.64/<0.0001
ID IV WM	0.0002/0.639	0.001/0.240	364.6/<0.0001*	−0.219/0.004*	72.12/<0.0001
Insula					
ID	0.0002/0.569	0.001/0.028	101.5/<0.0001*	0.148/0.252	17.78/<0.0001
ID IV	0.0001/0.691	<0.0001/0.940	146.9/<0.0001*	0.021/0.819	50.12/<0.0001
ID IV WM	0.0004/0.044	−<0.0001/0.955	410.2/<0.0001*	−0.368/0.0001*	68.45/<0.0001
Corpus callosum					
ID	0.002/0.038	0.002/0.107	11.49/0.762	0.101/0.193	1.951/<0.0001
ID IV	0.000/0.252	0.0002/0.816	196.3/<0.0001*	−0.045/0.347	39.11/<0.0001
ID IV WM	0.001/0.311	−<0.0001/0.974	205.1/<0.0001*	−0.081/0.101	38.38/<0.0001

In this analysis, we used the model as IC ≈ β1 * age + β2 * MMSE + β3 * diffusion index + β4 * WMV BTV index + ε (error). For the diffusion indices, we used ID, ID at IV, and ID_IV at WM. For the BTV index, we used WMV. Therefore, the three tested models were between ID and WMV, between ID_IV and WMV, and between ID_IV_WM and WMV for each ROI. For IC ROI data, $\alpha<0.05$ divided by 3 tested models (0.05/3=0.0166) was used to determine the significance level. *, significant association between conductivity value and other indices. ANOVA, analysis of variance; BTV, boundary tissue volume; IC, intra-neurite conductivity; ID, intra-neurite diffusivity; IV, intracellular volume; MMSE, Mini-Mental State Examination; ROI, region of interest; WM, white matter; WMV, white matter volume.

amygdala, thalamus, and insula when considered with certain diffusion indices. ID_IV and ID_IV_WM in the hippocampus and corpus callosum, and ID, ID_IV, and ID_IV_WM in the amygdala, thalamus, and insula, were significantly related to IC. Table S6 summarizes the analysis of IC_WM with diffusion metrics and WMV. The significance was confirmed across all ROIs. Age and MMSE scores were not significantly associated with IC_WM. WMV was meaningfully tied to IC_WM in the hippocampus, amygdala, thalamus, and insula regions. Diffusion indices ID_IV and ID_IV_WM in the hippocampus and corpus callosum, and ID, ID_IV, and ID_IV_WM in the amygdala, thalamus, and insula, showed significant association with IC_WM.

Discussion

To investigate how diffusivity impacts conductivity in the brain, and the influence of GMV, WMV, and CSF volume on brain conductivity, we applied MREPT and MC-SMT to calculate HFC and decomposed conductivities of EC and IC, along with diffusion indices in a cohort of 77 older individuals ranging from cognitively normal to cognitively impaired. The association results revealed that both HFC and EC demonstrate positive associations with diffusion indices such as ED, RD, MD, and AxD, but very little association with CSF volume (*Tables 2,3*). The association results also revealed that IC is positively associated with ID and WMV (*Table 4*). Furthermore, no significant

associations were observed between age or MMSE scores and any conductivity measures (*Tables 2-4*). Overall, the findings suggest that changes in diffusivity may be more critical in modeling conductivity alterations in various pathological conditions of the older brain. Diffusion is not sensitive to the presence and abundance of ions, whereas electrical properties tomography (EPT) will be very sensitive to that.

Impact of diffusion (mobility) on conductivity

Our results from multiple regression analyses underscore a significant positive relationship between brain conductivity measures (HFC, EC, IC, IC_WM, and EC_WM) and diffusion indices (*Tables 2-4*, Tables S5,S6), corroborating that electrical conductivity is indeed related to ion mobility as gauged by MRI-derived proton diffusion measurements.

HFC (*Table 2*) and EC (*Table 3*) exhibited positive associations with certain diffusion indices (MD, RD, AxD, and ED_EV) across the hippocampus and insula, potentially stemming from the extracellular compartment. This is consistent with previous research indicating that increased ion mobility, rather than ion concentration, accounts for elevated conductivity in AD patients (7,20,32). Despite hippocampal and insular atrophy potentially increasing CSF volume, loss of brain tissue did not significantly affect HFC or EC values, suggesting atrophy is not the main determinant of conductivity changes. Instead, cell density, with higher density reducing diffusivity, could be more influential on brain conductivity alterations. Furthermore, the positive correlation between EC and MD hints at extracellular fluid dynamics (13,33), where higher MD, indicating a less dense environment, facilitates ion movement, thus boosting conductivity. EC refers to the electrical conductivity of the space outside the neuronal axons, which includes the extracellular fluid (33). This fluid-filled space (13) allows ions to move relatively freely, contributing to the tissue's overall conductivity. MD is a measure of the overall mobility of water molecules, regardless of any preferential direction called isotropic diffusivity. The positive association between ED and MD can be understood in terms of the tissue microstructure: Higher MD indicates that water molecules are diffusing more freely, which is typically associated with a less dense or less structured environment. In the brain, this could mean less myelination or damage to the white matter tracts (34), resulting in more space for water and ions to move. If there is more free space in the extracellular environment (as suggested by higher MD) (13), ions can move more easily through the fluid, leading to increased conductivity. In essence, when the extracellular space is less restricted (higher MD), there is greater ionic mobility, which leads to higher EC. This relationship is particularly useful in understanding and diagnosing various neurological conditions where changes in tissue structure impact both diffusivity and conductivity (34-36).

The negative correlation observed between HFC or EC and FA underscores the nuanced relationship between white matter microstructure and conductivity (*Figure 3*): organized, myelinated white matter tracts limit ionic movement and, therefore, conductivity. This result indicates the same meaning as the positive correlation between HFC or EC and MD or ED. FA reflects the degree of directionality of water diffusion within the tissue, indicating diffusion anisotropy (37,38). EC, on the other hand, refers to the ability of the extra-neurite space (the space outside of neurons) to conduct electrical currents as we mentioned above. This space has low FA values with less restriction to the movement of ions and, therefore, has higher conductivity. The negative association between EC and FA can be explained by the microstructural environment of the brain's white matter (34,39,40). In areas where the white matter tracts are highly organized and myelinated (high FA) (34), the extracellular space is more restricted, which limits the movement of ions and reduces conductivity. Conversely, in areas with less myelination and organization (low FA), the extracellular space is more permissive, allowing for greater ionic movement and higher conductivity (38). Therefore, the relationship is such that a high FA area, indicating more organized white matter shows lower EC, indicating less space for ions to move freely (14). This inverse relationship helps in understanding the underlying microstructure and function of brain tissue and is valuable in the study of various neurological conditions (40,41). Conversely, less structured areas allow for increased diffusion and conductivity. This inverse relationship is essential for understanding brain tissue function and is valuable for neurological condition assessments. EC_WM was also positively linked to diffusivity (ED_EV_WM) across selected ROIs (Table S5, *Figure 3*), reflecting that structural properties conducive to water molecule movement similarly enhance ionic mobility, thus increasing conductivity.

Conversely, IC showed a positive connection with ID in the amygdala, thalamus, and insula (*Table 4*, *Figure 3*), illustrating that within the neuron, optimal conditions favor

both ion movement and diffusivity, with disease or damage impairing both (42). We expect that the IC signal, which is related to the ability of ions to move within the neuron, is mainly detected from the intra-neurite compartment, while intra-neurite or intracellular diffusivity refers to the movement of water molecules within the axons of neurons (36). The positive association between these two properties can be explained by the microstructural environment within the neurons (14). The interior of a neuron, particularly the axon, is a highly structured environment where both ions and water molecules are confined to a narrow space (43). This space is organized by the presence of microtubules, neurofilaments, and other cytoskeletal components. IC is influenced by the movement of ions across the neuronal membrane and along the axon (40). This movement is facilitated by various ion channels and pumps that regulate the flow of ions such as sodium, potassium, calcium, and chloride (44). ID is determined by how water molecules diffuse within the axon. This diffusion is restricted by the same structures that confine ions, leading to a directional movement known as anisotropic diffusion (38). When the intra-neurite space is healthy and intact, both ionic and water molecule movement are optimized, leading to higher conductivity and diffusivity. Conversely, if the intra-neurite environment is compromised (e.g., due to disease or damage) (36), both conductivity and diffusivity would decrease. Therefore, the positive association between IC and ID is due to the mutual dependence of ions and water molecules on the structural integrity and function of the intra-neurite environment. Negative correlations of IC with AxD, MD, RD, and ED further affirm this dependency on cellular integrity for both ionic and water molecule movement in brain tissue (*Figure 3*).

Our study supports the use of MREPT for measuring conductivity, emphasizing its reflection of ion mobility assessed by diffusion metrics. This complements previous studies that have explored the electrical properties of tissues using different MRI techniques (6,12,17-19,25,27,45,46). Highlight that the study's findings align with previous research on the independence of diffusion and conductivity as physiological parameters. A previous study found that the HFC conductivity value was negatively correlated with the apparent diffusion coefficient (ADC) value in patients with breast cancer (46). While diffusivity is typically restricted in breast cancer, it is not restricted in the brains of individuals with neurodegenerative diseases or aging brains. Therefore, a direct comparison between our study and the previous breast cancer study is not straightforward. In summary, this study supports our previous findings (7,20), which indicate that the elevated HFC and EC values in AD patients, compared to CN and MCI participants, can be attributed to increased ion mobility, measured as isotropic diffusivity, rather than to increased ion concentration, measured as brain tissue volume loss. Imaging the electrical properties of biological tissues is a complex process because conductivity in the human body varies due to various physiological conditions, including ion mobility, ion concentration, cell shapes, and cell membranes. Therefore, the correlation between conductivity and diffusivity in physiological processes is not automatically governed by physical laws. Previous studies have found that diffusion and conductivity are physically independent parameters (12,47).

It reveals that MREPT-derived conductivity measurements are predominantly influenced by the mobility of protons, as assessed by diffusion metrics. As we mentioned before, diffusion probes the mobility of protons whereas electrical conductivity probes the mobility of charged ions such as sodium ions. These two mobilities are different. To provide convincing evidence that both are closely associated, some realistic simulations at Larmor frequency would be needed by creating a realistic tissue environment of the brain and simulating diffusion and by adding ions such as sodium or potassium. He *et al.* performed a phantom study to investigate the relationship between conductivity and the diffusion time of an open-ended coaxial probe (48). Conductivity was slightly decreased with increasing the diffusion time.

Electrical impedance tomography (EIT) is a technique that images the electrical properties of tissues by applying small electrical currents and measuring the resulting voltages on the body's surface (17,49). At low frequencies (up to a few kHz), the current cannot pass through the membranes and primarily flows through the extracellular space because the cell membranes act as insulators. This results in higher impedance due to the dominance of extracellular resistance and membrane capacitance. At intermediate frequencies (a few kHz to MHz), the capacitive reactance of the cell membranes decreases, allowing more current to pass through the cells. This reduces the overall impedance. At high frequencies (MHz and above), the current will then be able to pass more easily through the cell membrane, and the impedance is mainly determined by the intracellular and extracellular resistances. The overall impedance decreases significantly, indicating that the overall conductivity of the tissues will be higher.

Influence of brain tissue volume on conductivity

The multiple regression analysis in our study indicates that while neither HFC nor EC correlates significantly with overall brain tissue volumes, both conductivities within white matter (EC_WM, IC_WM) and IC positively correlate with the volume of white matter (*Tables 2-4*). This suggests that the integrity and volume of white matter play a crucial role in determining IC.

We found no significant relationship between HFC, EC, and the volume of CSF, contrary to initial expectations that CSF volume would heavily influence these conductivity values, especially since they are measured mainly in extracellular areas (*Tables 2,3*). This lack of association suggests the properties defining conductivity in these compartments differ. The mechanics of CSF movement do not directly interact with the parenchyma's electrical properties, which include both neuronal and extracellular conductivities (13,36).

We found positive correlations between EC_WM and WMV in the hippocampus and thalamus (Table S5). White matter in the brain primarily consists of myelinated axons, which are the long projections of neurons that transmit electrical signals across different parts of the brain. Myelin is a fatty substance that insulates these axons and significantly increases the speed and efficiency of electrical signal transmission. Similarly, IC shows a positive relationship with WMV in the hippocampus and thalamus (*Table 4*), indicating that a higher volume of well-myelinated axons leads to improved electrical signal propagation within neurons.

Correlation between conductivity and MMSE scores and age

Voxel-based analysis revealed a negative correlation between conductivity measures (HFC, EC, and EC_WM) and MMSE scores (*Figure 2*), localized specifically to the insula (*Table 1*). However, our multiple regression model showed that neither age nor MMSE scores were significant predictors of conductivity indices across all ROIs (*Tables 2-4*).

The insula is highly susceptible to cerebral atrophy, and patients with lower MMSE scores, indicative of more advanced cognitive decline, typically exhibit increased diffusivity in this region (50). This pattern reflects the negative correlation we observed between MMSE scores and both HFC and EC. Our findings align with those from previous research on AD (7,51), emphasizing that increased diffusivity—a marker for the ease of water molecule movement in tissue—is common in individuals with cognitive impairments, including AD and mild cognitive impairment (MCI) as reported by Jahng *et al.* (51,52).

Contrary to expectations, we did not find a significant connection between conductivity and MMSE scores in the hippocampus, often considered a key area affected in AD (53). Previous studies, including the one by Park *et al.* (7), also reported no notable association between hippocampal HFC and cognitive function. It's uncertain whether the sensitivity of our conductivity measurements lacks the granularity to detect subtle levels of cognitive impairment. As such, further investigation is warranted to validate these observations and to delve into the mechanisms at play.

Although no significant associations were observed between age and any conductivity measures (*Tables 2-4*), we found that HFC values in the white matter decreased with increasing age (*Table 2*). A previous study reported that the HFC conductivity value in the white matter increased with age due to the rising brain water content (19,54). In that study, the 17 healthy volunteers (10 males and 7 females) were aged between 25 and 73 (43.5±16.9) years old. He *et al.* found a conductivity increase of 0.002 S/m per year (19). The rate of conductivity reduction per year was consistent with the findings of the previous study (*Table 2*, corpus callosum). The lack of significant correlations between age and conductivity measures in MREPT studies can be attributed to several potential confounding factors. First, our current study included a cohort of 77 older individuals, aged 74.9±5.8 years, with a male-to-female ratio of 24:53. This narrow range of age may not capture the full spectrum of age-related changes. Including a broader range of age might reveal more significant associations by accounting for variability in aging effects. A previous study found that HFC in white matter increased with age due to rising brain water content (7). Second, hydration levels, which affect brain water content, might confound the relationship between age and conductivity (55). Variations in hydration levels among individuals can significantly affect tissue conductivity. Well-hydrated tissues generally exhibit higher conductivity due to the increased presence of free water molecules that facilitate ion movement. Aging can lead to changes in body water content, with older adults often experiencing reduced hydration levels (56-58). This variability can obscure the relationship between age and conductivity measures. Third, the concentration of ions such as sodium, potassium, and chloride in tissues influences conductivity. Individual differences in diet, health status, and medication use can lead

to variations in ion concentration, affecting conductivity measurements (59). Research indicates that aging can lead to imbalances in these metal ions, contributing to cognitive decline and other neurological issues (60). Since conductivity is influenced by the movement of ions, variations in hydration levels and ion concentrations could obscure age-related changes in conductivity.

Influence diagnostic or therapeutic strategies

Our findings necessitate further exploration into the mechanisms by which conductivity is altered in the aging brain and neurodegenerative diseases, potentially leading to the identification of new biomarkers (61). The study demonstrates that conductivity measurements derived from MREPT are primarily reflective of ion mobility, which can be correlated with microstructural changes in brain tissue. This suggests that MREPT could be a valuable diagnostic tool for detecting early changes in brain structure associated with aging and neurodegenerative diseases like AD. The ability to measure specific conductivity changes in different brain regions can help differentiate between types of neurodegenerative diseases based on distinct conductivity profiles. For instance, variations in conductivity within the insula and other regions could help identify specific patterns associated with cognitive decline (7,20,51). Understanding the relationship between conductivity and tissue microstructure could guide the development of targeted therapies that aim to preserve or restore tissue integrity, potentially slowing the progression of neurodegenerative diseases. Conductivity measurements could be used to monitor the efficacy of therapeutic interventions by providing a quantitative measure of changes in brain tissue over time, thereby assessing treatment impact on ion mobility and diffusion properties (62). The findings highlight the need for further research into the mechanisms linking conductivity changes to cognitive decline, which could lead to the discovery of new biomarkers for early diagnosis and intervention.

Limitations

This study has several limitations worth noting. Firstly, the sample size was relatively small, which may restrict the generalizability of our findings. In addition, we only included elderly participants in this study. Therefore, in a future study, we recommend including young participants. Secondly, the investigation was conducted within a single center, introducing a potential risk for selection bias. Future research should extend to larger, more diverse populations and adopt a multi-center approach to mitigate these issues. Thirdly, due to the modest number of participants, we selected specific diffusion and brain tissue volume indices to evaluate conductivity in our multiple regression models. Future research should employ more robust and comprehensive modeling techniques to explore these relationships further.

Fourth, the six-echo TSE sequence has a scan time of approximately 6 minutes and 5 seconds. While this duration is relatively short for comprehensive brain imaging, it can still be challenging for elderly participants, who may have difficulty remaining still for extended periods. Elderly individuals might experience discomfort or fatigue during prolonged scans, which could lead to motion artifacts and affect the quality of the images. The use of a multi-echo sequence like the six-echo TSE can improve image quality by providing multiple echoes for analysis, enhancing the signal-to-noise ratio and allowing for more detailed conductivity mapping. However, this comes at the cost of longer scan times, which can be particularly taxing for older adults. Currently, we are trying to optimize the TSE sequence for faster acquisition using the compressed parallel imaging technique with artificial intelligence.

Fifth, we recognized that using BTVs as proxies for proton density is a simplification that may not accurately reflect ion concentrations. BTVs derived from MRI, such as GMV, WMV, and CSF volume, are typically inferred from T1-weighted images and may not capture the nuanced variations in ion concentrations. The use of sodium MRI is a more direct method to map ion concentrations (11). Unlike proton MRI, which reflects proton concentration indirectly through tissue volumes, sodium MRI can provide explicit measurements of sodium ion distribution, offering a clearer picture of the ionic environment in the brain (63,64). Future studies should incorporate sodium MRI to validate the relationship between conductivity and ion concentrations, particularly in pathological states like neurodegenerative diseases and aging brains (11).

Sixth, we employed the MC-SMT diffusion model to disaggregate HFC into EC and IC. We recommend additional studies to confirm the validity and reliability of these decomposed components. Finally, the assumption of a direct relationship between ion concentration and brain tissue volumes requires further clarification. Since the ratio β in Eq. [6] depends on the ion concentration and brain tissue volumes, β cannot be fixed as a constant

in the whole brain region. However, no method to experimentally estimate the ratio of ion concentrations in the intra- and extra-compartments of the human brain is available, therefore, we used the ratio value β=0.41, which is a reference value suggested by studies of intracellular and extracellular ion concentrations of four predominant ions including Na^+, Cl^-, K^+, and Ca^+ (20). Although sodium MRI is not frequently used in clinical settings, we believe that it provides the best representation of ion concentration in MRI experiments. Therefore, future studies should focus on investigating the association between conductivity and ion concentration measured with sodium MRI, rather than brain tissue volume, in aging brains and patients with neurodegenerative diseases.

Conclusions

This study explored the relationships between HFC and its subcomponents—EC and IC—and various brain tissue characteristics such as volume and diffusivity in the aging brain. Our findings suggest that HFC and EC are statistically correlated with diffusion indices including MD, RD, and AxD. Notably, no correlations were observed between HFC or EC and CSF volume. Within white matter, EC exhibited associations with both white matter diffusivity and WMV. Similarly, IC correlated with the ID index and WMV. These results imply that conductivity measurements derived from MREPT are primarily reflective of ion mobility, as assessed by diffusion metrics, with lesser contributions from tissue proton density, as suggested by segmented brain tissue volumes. These findings imply that clinical interpretations of MREPT data require careful consideration to distinguish between changes due to conductivity from those related to diffusion. This distinction is vital to ensure the accuracy of diagnostic conclusions.

Acknowledgments

The authors appreciate Miss Seon Hwa Lee (Clinical Research Institute, Kyung Hee University Hospital at Gangdong, Seoul, Republic of Korea) for providing advice on the statistical analyses.

Footnote

Reporting Checklist: The authors have completed the STROBE reporting checklist. Available at https://qims.amegroups.com/article/view/10.21037/qims-24-2145/rc

Funding: The research was supported by the National Research Foundation of Korea (NRF) grants funded by the Ministry of Science and ICT (No. RS-2024-00335770 to G.H.J.; No. RS-2023-00250977 to M.B.L.).

Conflicts of Interest: All authors have completed the ICMJE uniform disclosure form (available at https://qims.amegroups.com/article/view/10.21037/qims-24-2145/coif). M.B.L. reports funding from the National Research Foundation of Korea (NRF) grants funded by the Ministry of Science and ICT (No. RS-2023-00250977). G.H.J. reports funding from the National Research Foundation of Korea (NRF) grants funded by the Ministry of Science and ICT (No. RS-2024-00335770). The other authors have no conflicts of interest to declare.

Ethical Statement: The authors are accountable for all aspects of the work in ensuring that questions related to the accuracy or integrity of any part of the work are appropriately investigated and resolved. The study was conducted in accordance with the Declaration of Helsinki and its subsequent amendments. The study was approved by the Institutional Review Board (IRB) of Kyung Hee University Hospital at Gangdong, Seoul, Republic of Korea (IRB No. khnmc2019-07-007), and all participants provided informed consent before their inclusion in this cross-sectional prospective study.

References

1. Newnham RE. Properties of materials: anisotropy, symmetry, structure. Oxford University Press; 2005.
2. Katscher U, Voigt T, Findeklee C, Vernickel P, Nehrke K, Dössel O. Determination of electric conductivity and local SAR via B1 mapping. IEEE Trans Med Imaging 2009;28:1365-74.

3. Akhtari M, Salamon N, Duncan R, Fried I, Mathern GW. Electrical conductivities of the freshly excised cerebral cortex in epilepsy surgery patients; correlation with pathology, seizure duration, and diffusion tensor imaging. Brain Topogr 2006;18:281-90.
4. Frantseva M, Cui J, Farzan F, Chinta LV, Perez Velazquez JL, Daskalakis ZJ. Disrupted cortical conductivity in schizophrenia: TMS-EEG study. Cereb Cortex 2014;24:211-21.
5. Haemmerich D, Schutt DJ, Wright AW, Webster JG, Mahvi DM. Electrical conductivity measurement of excised human metastatic liver tumours before and after thermal ablation. Physiol Meas 2009;30:459-66.
6. Kim SY, Shin J, Kim DH, Kim MJ, Kim EK, Moon HJ, Yoon JH. Correlation between conductivity and prognostic factors in invasive breast cancer using magnetic resonance electric properties tomography (MREPT). Eur Radiol 2016;26:2317-26.
7. Park S, Jung SM, Lee MB, Rhee HY, Ryu CW, Cho AR, Kwon OI, Jahng GH. Application of High-Frequency Conductivity Map Using MRI to Evaluate It in the Brain of Alzheimer's Disease Patients. Front Neurol 2022;13:872878.
8. Tha KK, Katscher U, Yamaguchi S, Stehning C, Terasaka S, Fujima N, Kudo K, Kazumata K, Yamamoto T, Van Cauteren M, Shirato H. Noninvasive electrical conductivity measurement by MRI: a test of its validity and the electrical conductivity characteristics of glioma. Eur Radiol 2018;28:348-55.
9. Kaden E, Kelm ND, Carson RP, Does MD, Alexander DC. Multi-compartment microscopic diffusion imaging. Neuroimage 2016;139:346-59.
10. Zhang H, Schneider T, Wheeler-Kingshott CA, Alexander DC. NODDI: practical in vivo neurite orientation dispersion and density imaging of the human brain. Neuroimage 2012;61:1000-16.
11. Liao Y, Lechea N, Magill AW, Worthoff WA, Gras V, Shah NJ. Correlation of quantitative conductivity mapping and total tissue sodium concentration at 3T/4T. Magn Reson Med 2019;82:1518-26.
12. Katscher U, van den Berg CAT. Electric properties tomography: Biochemical, physical and technical background, evaluation and clinical applications. NMR Biomed 2017.
13. Hrabetova S, Cognet L, Rusakov DA, Nägerl UV. Unveiling the Extracellular Space of the Brain: From Super-resolved Microstructure to In Vivo Function. J Neurosci 2018;38:9355-63.
14. McCann H, Pisano G, Beltrachini L. Variation in Reported Human Head Tissue Electrical Conductivity Values. Brain Topogr 2019;32:825-58.
15. Kulbacka J, Choromańska A, Rossowska J, Wężgowiec J, Saczko J, Rols MP. Cell Membrane Transport Mechanisms: Ion Channels and Electrical Properties of Cell Membranes. Adv Anat Embryol Cell Biol 2017;227:39-58.
16. Li Y, Sun SX. The influence of polarized membrane ion carriers and extracellular electrical/pH gradients on cell ionic homeostasis and locomotion. bioRxiv 2023. doi: 10.1101/2023.07.26.550658.
17. Adler A, Boyle A. Electrical Impedance Tomography: Tissue Properties to Image Measures. IEEE Trans Biomed Eng 2017;64:2494-504.
18. Cao J, Ball I, Humburg P, Dokos S, Rae C. Repeatability of brain phase-based magnetic resonance electric properties tomography methods and effect of compressed SENSE and RF shimming. Phys Eng Sci Med 2023;46:753-66.
19. He Z, Soullié P, Lefebvre P, Ambarki K, Felblinger J, Odille F. Changes of in vivo electrical conductivity in the brain and torso related to age, fat fraction and sex using MRI. Sci Rep 2024;14:16109.
20. Hong S, Choi Y, Lee MB, Rhee HY, Park S, Ryu CW, Cho AR, Kwon OI, Jahng GH. Increased extra-neurite conductivity of brain in patients with Alzheimer's disease: A pilot study. Psychiatry Res Neuroimaging 2024;340:111807.
21. Sengoku R. Aging and Alzheimer's disease pathology. Neuropathology 2020;40:22-9.
22. Breijyeh Z, Karaman R. Comprehensive Review on Alzheimer's Disease: Causes and Treatment. Molecules 2020;25:5789.
23. Ahn HJ, Chin J, Park A, Lee BH, Suh MK, Seo SW, Na DL. Seoul Neuropsychological Screening Battery-dementia version (SNSB-D): a useful tool for assessing and monitoring cognitive impairments in dementia patients. J Korean Med Sci 2010;25:1071-6.
24. Mandija S, Petrov PI, Vink JJT, Neggers SFW, van den Berg CAT. Brain Tissue Conductivity Measurements with MR-Electrical Properties Tomography: An In Vivo Study. Brain Topogr 2021;34:56-63.
25. Gurler N, Ider YZ. Gradient-based electrical conductivity imaging using MR phase. Magn Reson Med 2017;77:137-50.
26. Liu J, Wang Y, Katscher U, He B. Electrical Properties Tomography Based on B1 Maps in MRI: Principles, Applications and Challenges. IEEE Trans Biomed Eng 2017;64:2515-30.
27. Choi BK, Katoch N, Kim HJ, Park JA, Ko IO, Kwon OI,

Woo EJ. Validation of conductivity tensor imaging using giant vesicle suspensions with different ion mobilities. Biomed Eng Online 2020;19:35.
28. Jahng GH, Lee MB, Kim HJ, Je Woo E, Kwon OI. Low-frequency dominant electrical conductivity imaging of in vivo human brain using high-frequency conductivity at Larmor-frequency and spherical mean diffusivity without external injection current. Neuroimage 2021;225:117466.
29. Marino M, Cordero-Grande L, Mantini D, Ferrazzi G. Conductivity Tensor Imaging of the Human Brain Using Water Mapping Techniques. Front Neurosci 2021;15:694645.
30. Sajib SZK, Kwon OI, Kim HJ, Woo EJ. Electrodeless conductivity tensor imaging (CTI) using MRI: basic theory and animal experiments. Biomed Eng Lett 2018;8:273-82.
31. Guo XY, Chang Y, Kim Y, Rhee HY, Cho AR, Park S, Ryu CW, San Lee J, Lee KM, Shin W, Park KC, Kim EJ, Jahng GH. Development and evaluation of a T1 standard brain template for Alzheimer disease. Quant Imaging Med Surg 2021;11:2224-44.
32. Zerbi V, Kleinnijenhuis M, Fang X, Jansen D, Veltien A, Van Asten J, Timmer N, Dederen PJ, Kiliaan AJ, Heerschap A. Gray and white matter degeneration revealed by diffusion in an Alzheimer mouse model. Neurobiol Aging 2013;34:1440-50.
33. Soria FN, Miguelez C, Peñagarikano O, Tønnesen J. Current Techniques for Investigating the Brain Extracellular Space. Front Neurosci 2020;14:570750.
34. Khelfaoui H, Ibaceta-Gonzalez C, Angulo MC. Functional myelin in cognition and neurodevelopmental disorders. Cell Mol Life Sci 2024;81:181.
35. Newman BT, Jacokes Z, Venkadesh S, Webb SJ, Kleinhans NM, McPartland JC, Druzgal TJ, Pelphrey KA, Van Horn JD; GENDAAR Research Consortium. Conduction velocity, G-ratio, and extracellular water as microstructural characteristics of autism spectrum disorder. PLoS One 2024;19:e0301964.
36. Clements RT, Fuller LE, Kraemer KR, Radomski SA, Hunter-Chang S, Hall WC, Kalantar AA, Kraemer BR. Quantification of Neurite Degeneration with Enhanced Accuracy and Efficiency in an In Vitro Model of Parkinson's Disease. eNeuro 2022;9:ENEURO.
37. McDonough IM, Siegel JT. The Relation Between White Matter Microstructure and Network Complexity: Implications for Processing Efficiency. Front Integr Neurosci 2018;12:43.
38. Hansen MB, Jespersen SN, Leigland LA, Kroenke CD. Using diffusion anisotropy to characterize neuronal morphology in gray matter: the orientation distribution of axons and dendrites in the NeuroMorpho.org database. Front Integr Neurosci 2013;7:31.
39. Ritchie SJ, Bastin ME, Tucker-Drob EM, Maniega SM, Engelhardt LE, Cox SR, Royle NA, Gow AJ, Corley J, Pattie A, Taylor AM, Valdés Hernández Mdel C, Starr JM, Wardlaw JM, Deary IJ. Coupled changes in brain white matter microstructure and fluid intelligence in later life. J Neurosci 2015;35:8672-82.
40. Schilling KG, Chad JA, Chamberland M, Nozais V, Rheault F, Archer D, Li M, Gao Y, Cai L, Del'Acqua F, Newton A, Moyer D, Gore JC, Lebel C, Landman BA. White matter tract microstructure, macrostructure, and associated cortical gray matter morphology across the lifespan. bioRxiv. 2023. doi: 10.1101/2023.09.25.559330.
41. Raghavan S, Reid RI, Przybelski SA, Lesnick TG, Graff-Radford J, Schwarz CG, Knopman DS, Mielke MM, Machulda MM, Petersen RC, Jack CR Jr, Vemuri P. Diffusion models reveal white matter microstructural changes with ageing, pathology and cognition. Brain Commun 2021;3:fcab106.
42. Hu H, Klug J, Dietz M. Simulation of ITD-Dependent Single-Neuron Responses Under Electrical Stimulation and with Amplitude-Modulated Acoustic Stimuli. J Assoc Res Otolaryngol 2022;23:535-50.
43. Beebe NL, Young JW, Mellott JG, Schofield BR. Extracellular Molecular Markers and Soma Size of Inhibitory Neurons: Evidence for Four Subtypes of GABAergic Cells in the Inferior Colliculus. J Neurosci 2016;36:3988-99.
44. Chu YH, Lin JD, Nath S, Schachtrup C. Id proteins: emerging roles in CNS disease and targets for modifying neural stemcell behavior. Cell Tissue Res 2022;387:433-49.
45. Kim S, Choi BK, Park JA, Kim HJ, Oh TI, Kang WS, Kim JW, Park HJ. Identification of Brain Damage after Seizures Using an MR-Based Electrical Conductivity Imaging Method. Diagnostics (Basel) 2021.
46. Kim SY, Shin J, Kim DH, Kim EK, Moon HJ, Yoon JH, You JK, Kim MJ. Correlation between electrical conductivity and apparent diffusion coefficient in breast cancer: effect of necrosis on magnetic resonance imaging. Eur Radiol 2018;28:3204-14.
47. Gho SM, Shin J, Kim MO, Kim MJ, Kim S, Kim JH, Kim DH. Observation of the correlation between electrical conductivity and apparent diffusion coefficient values. Proceedings of the 24th Annual Meeting ISMRM; 2016; Milan, Italy. 2016;1566.

48. He Z, Lefebvre PM, Soullié P, Doguet M, Ambarki K, Chen B, Odille F. Phantom evaluation of electrical conductivity mapping by MRI: Comparison to vector network analyzer measurements and spatial resolution assessment. Magn Reson Med 2024;91:2374-90.
49. Mansouri S, Alharbi Y, Haddad F, Chabcoub S, Alshrouf A, Abd-Elghany AA. Electrical Impedance Tomography - Recent Applications and Developments. J Electr Bioimpedance 2021;12:50-62.
50. Moon Y, Moon WJ, Han SH. Pathomechanisms of atrophy in insular cortex in Alzheimer's disease. Am J Alzheimers Dis Other Demen 2015;30:497-502.
51. Kwon OI, Jahng GH, Lee M. Texture Analyses of Electrical Conductivity Maps in the Insula of Alzheimer's Disease Patients. J Med Biol Eng 2024;44:208-19.
52. Jahng GH, Xu S, Weiner MW, Meyerhoff DJ, Park S, Schuff N. DTI studies in patients with Alzheimer's disease, mild cognitive impairment, or normal cognition with evaluation of the intrinsic background gradients. Neuroradiology 2011;53:749-62.
53. Zhang J, Xie L, Cheng C, Liu Y, Zhang X, Wang H, Hu J, Yu H, Xu J. Hippocampal subfield volumes in mild cognitive impairment and alzheimer's disease: a systematic review and meta-analysis. Brain Imaging Behav 2023;17:778-93.
54. Stetson DS, Albers JW, Silverstein BA, Wolfe RA. Effects of age, sex, and anthropometric factors on nerve conduction measures. Muscle Nerve 1992;15:1095-104.
55. Pappas C, Bauer CE, Zachariou V, Maillard P, Caprihan A, Shao X, Wang DJJ, Gold BT. MRI free water mediates the association between water exchange rate across the blood brain barrier and executive function among older adults. Imaging Neurosci (Camb) 2024;2:1-15.
56. Wittbrodt MT, Sawka MN, Mizelle JC, Wheaton LA, Millard-Stafford ML. Exercise-heat stress with and without water replacement alters brain structures and impairs visuomotor performance. Physiol Rep 2018;6:e13805.
57. Masento NA, Golightly M, Field DT, Butler LT, van Reekum CM. Effects of hydration status on cognitive performance and mood. Br J Nutr 2014;111:1841-52.
58. Nishi SK, Babio N, Paz-Graniel I, Serra-Majem L, Vioque J, Fitó M, et al. Water intake, hydration status and 2-year changes in cognitive performance: a prospective cohort study. BMC Med 2023;21:82.
59. Strickland M, Yacoubi-Loueslati B, Bouhaouala-Zahar B, Pender SLF, Larbi A. Relationships Between Ion Channels, Mitochondrial Functions and Inflammation in Human Aging. Front Physiol 2019;10:158.
60. Singh R, Panghal A, Jadhav K, Thakur A, Verma RK, Singh C, Goyal M, Kumar J, Namdeo AG. Recent Advances in Targeting Transition Metals (Copper, Iron, and Zinc) in Alzheimer's Disease. Mol Neurobiol 2024;61:10916-40.
61. Lee J, Kim HJ. Normal Aging Induces Changes in the Brain and Neurodegeneration Progress: Review of the Structural, Biochemical, Metabolic, Cellular, and Molecular Changes. Front Aging Neurosci 2022;14:931536.
62. Benchakroun H, Ištuk N, Dunne E, Elahi MA, O'Halloran T, O'Halloran M, O'Loughlin D. Probe Contact Force Monitoring during Conductivity Measurements of the Left Atrial Appendage to Support the Design of Novel Diagnostic and Therapeutic Procedures. Sensors (Basel) 2022.
63. Hagiwara A, Bydder M, Oughourlian TC, Yao J, Salamon N, Jahan R, Villablanca JP, Enzmann DR, Ellingson BM. Sodium MR Neuroimaging. AJNR Am J Neuroradiol 2021;42:1920-6.
64. Huhn K, Engelhorn T, Linker RA, Nagel AM. Potential of Sodium MRI as a Biomarker for Neurodegeneration and Neuroinflammation in Multiple Sclerosis. Front Neurol 2019;10:84.

Cite this article as: Park T, Choi Y, Kwon HJ, Lee MB, Rhee HY, Park S, Ryu CW, Jahng GH. Exploring the relationship between larmor-frequency electrical conductivity, diffusivity, and tissue volume in the aging brain. Quant Imaging Med Surg 2025;15(5):4669-4688. doi: 10.21037/qims-24-2145